Plasmonics (2020) 15:1489–1498
https://doi.org/10.1007/s11468-020-01165-z

Highly Sensitive SPR Sensor Based on Ag-ITO-BlueP/TMDCs-Graphene Heterostructure

Lei Han[1] · Huafeng Ding[1] · Ngaleu Nematchoa Adrien Landry[1] · Menghu Hua[1] · Tianye Huang[1]

Received: 14 November 2019 / Accepted: 31 March 2020 / Published online: 22 April 2020

Abstract
The novel surface plasmon resonance (SPR) sensor based on hybrid structure of Ag-indium tin oxide (ITO)-blue phosphorene (BlueP)/transition metal dichalcogenides (TMDCs)-graphene is presented. The BlueP/TMDCs heterostructure works as an interacting layer with the analyte for the enhancement of the of the sensor's sensitivity. For angular sensitivity, when the BlueP/WS_2 and graphene are both monolayer, the highest angular sensitivity with 348.8°/RIU is obtained. The maximum angular sensitivity of our proposed SPR sensor is about 2.83 times of the conventional sensor. For phase sensitivity, when the BlueP/WSe_2 is monolayer and graphene is bilayer, the highest phase sensitivity with 3.603×10^6 deg/RIU is obtained. The highest phase sensitivity of our proposed SPR sensor is about 2.78 times of the Ag-ITO-graphene structure and 4.16 times of the Ag-ITO structure. The SPR sensor has the advantages of high sensitivity, repeatability, and reusability, so it has a good prospect application for food safety detection, biological engineering, medical diagnosis, and biochemical detection.

Keywords Blue phosphorene · Transition metal dichalcogenides · Graphene · Indium tin oxide · Surface plasmon resonance · Sensitivity

Introduction

Surface plasmon (SP) wave is sensitive to the change of the refractive index of the sensing medium, and the application of surface plasmon resonance (SPR) in sensor has attracted extensive attention and research. Based on this mechanism, different types of SPR sensor are designed to detect analysis. SPR sensor is a new biochemical detection technology, which has many advantages, such as high sensitivity, convenient detection, and online detection [1–4]. It can be widely used in many fields, such as material science, environmental protection, and food industry, which are directly related to human survival and development [5–8]. In order to improve the performance of SPR, many researchers have studied new materials [9, 10] and incident light in different wavelength [11, 12] and optimized the structure [13, 14].

The traditional SPR sensor is a Kretschmann prism coupling structure, which is no gap between the prism and the metal film. The metal film is directly covered on the bottom of the prism, and the object under test is placed under the metal film. A beam of monochromatic polarized light is transmitted through the prism, and the SPR phenomenon is excited by changing the incident angle θ of the incident light or changing the wavelength λ [15]. In the traditional SPR sensor, gold (Au) [16], silver (Ag) [17, 18], aluminum (Al) [19], and copper (Cu) [20] are commonly used as plasma metals. Ag has better properties than other metals, so it is widely used in SPR sensor. Leong et al. prepared the Ag nanoparticles to have high uniformity and uniformity, which opens up a way for SPR to effectively utilize the visible light region of electromagnetic spectrum [21]. Osov et al. investigated the optical and morphological properties of CsBr-Ag complex thin films deposited by thermal evaporation on glass substrate [22].

The metal layer of traditional SPR sensor usually uses precious metals, such as Au and Ag. It has been found that indium tin oxide (ITO) can replace precious metals to produce surface plasmons, so how to use ITO to excite SPR has attracted the researcher's attention [23, 24]. ITO film has good conductivity, high transmission to visible light, and high reflection to infrared light [25–27]. Li et al. designed a self-reference bimodal SPR sensor based on Au/ITO nanocomposite [28]. Szunertis et al. prepared ITO thin films by radio frequency sputtering at room temperature and prepared Ag/ITO and U/ITO interfaces in chemical and optical stability

✉ Tianye Huang
tianye_huang@163.com

[1] School of Mechanical Engineering and Electronic Information, China University of Geosciences (Wuhan), Wuhan 430074, China

[29]. Huang et al. proposed a vertical stack silica-silicon-HfO_2-ITO-HfO_2-Ag-prism multilayer light reflection modulator based on SPR and studied it numerically [13]. Gan et al. proposed a SPR sensor based on chromium-Ag-ITO structure with sensitivity up to 69.88°/RIU [30]. Sharma et al. proposed a sensitive quartz glass prism SPR sensor with ITO layer and obtained the sensitivity of 164°/RIU [31].

Since the first discovery of two-dimensional (2D) materials in 2004, 2D materials have attracted wide attention [32]. Graphene is one of the most widely used 2D materials [33], which is only composed of a single hexagonal arrangement of carbon atoms, with ultra-high electron mobility [34]. Simsek et al. proved theoretically and numerically that graphene can improve the tuning range and sensitivity of SPR biosensor [35]. Chiu et.al proposed a high-sensitivity immunoassay sensor for graphene oxide chip-based SPR chips [36]. Said et al. proposed a finite difference time domain method to study the effect of graphene as a monolayer coating on the surface of Ag, Au, Al, Cu, and other metal films [37]. With the discovery of graphene, some new 2D materials black phosphorus (BP) and transition metal dichalcogenides (TMDCs) have been widely used in transistors and photodetectors due to their high carrier mobility and excellent optical and electrical properties [38, 39]. For the angular sensitivity, Ouyang et al. designed SPR biosensor with Au-silicon-WS_2, which the highest sensitivity reached to 155.68°/RIU [40]. Meshginqalam et al. compared the different biosensor structures based on a small amount of 2D materials such as BP with the sensor parameters of traditional Au-based SPR biosensor. The maximum angular sensitivity of the structure consisting of 10-layer BP and monolayer WS_2 was 187°/RIU [41]. Han et al. proposed that the maximum angular sensitivity of SPR biosensor based on Ag-ITO-WS_2 structures is 219.4°/RIU [42]. Wu et al. designed SPR biosensor by using few-layer BP and TMDCs heterostructure, which improved the sensitivity of the sensor, and the highest sensitivity was 279°/RIU [43]. Zhao et al. obtained the maximum angular sensitivity (315.5°/RIU) with WS_2 (7-layers)-Al-WS_2 (7-layers)-graphene structure [44]. For the phase sensitivity, Zeng et al. developed SPR biosensor with high sensitive with Au-graphene-MoS_2 structure, which phase sensitivity of 8.185×10^4 deg/RIU is obtained [45]. Han et al. proposed that the maximum phase sensitivity of SPR biosensor based on Ag-ITO-WS_2 structures is 1.711×10^6 deg/RIU [46]. Huang et al. proposed that the highest phase sensitivity based on Cu-ITO-$MoSe_2$ dielectric structure is 1.821×10^6 deg/RIU [42]. In addition, owing to the fact that both blue phosphorene (BlueP) and TMDCs monolayer have same hexagonal crystal structure, the hybrid structure of BlueP/TMDCs can be constructed [47]. In the results shown that compared with the traditional SPR sensor, the sensitivity of the BlueP/MoS_2 heterostructure is increased from 150.66°/RIU to 230.66°/RIU [48]. In order to enhance the sensitivity of traditional SPR sensor and utilize the advantageous properties of BlueP/TMDCs, a hybrid structure based on Ag-ITO-BlueP/TMDCs-graphene is proposed. The results show that ITO, BlueP/TMDCs, and graphene can be combined to enhance the performance.

Design Configuration and Theoretical Method

In Fig. 1a, the angular sensitivity of SPR sensor comprises six layers based on the Kretschmann configuration. As the coupling prism, the BK7 glass is used for SPR sensor and its refractive index is determined by the following relation [49]:

$$n_{A1} = \sqrt{\frac{1.03961212\lambda^2}{\lambda^2 - 0.00600069867} + \frac{0.231792344\lambda^2}{\lambda^2 - 0.0200179144} + \frac{1.01046945\lambda^2}{\lambda^2 - 103.560653} + 1} \quad (1)$$

where λ is the wavelength of incident light in μm. The refractive index of the second layer of silver (Ag) film can be calculated by the following formula based on the Drude-Lorentz model [50]:

$$n_{A2} = \sqrt{1 - \frac{\gamma_c \lambda^2}{\gamma_p^2 (\gamma_c + i\lambda)}} \quad (2)$$

where γ_p (1.4541×10^{-7} m) and γ_c (1.7614×10^{-7} m) denote the plasma and collision wavelength. For the third layer of ITO film, it can be described quantitatively by the classical Drude free-electron theory [51]:

$$n_{A3} = \sqrt{3.8 - \frac{\gamma_c \lambda^2}{\gamma_p^2 (\gamma_c + i\lambda)}} \quad (3)$$

where γ_p and γ_c are 0.56497×10^{-7} m and 11.21076×10^{-7} m, respectively. The fourth layer of BlueP/TMDCs with the monolayer and refractive index at $\lambda = 632.8$ nm are shown as Table 1 [47, 48]. Finally, the refractive index of the fifth layer of graphene in the visible light range is given as [51]:

$$n_{A5} = 3.0 + i\frac{C_1}{3}\lambda \quad (4)$$

where the constant $C_1 \approx 5.446 \times 10^{-7}$ m and the monolayer thickness of graphene is 0.34 nm. The sensing medium used for initial calibration is deionized water with a refractive index of $n_{A6} = 1.330 + \Delta n$ [46]. Using Δn expressed the change of the refractive index of the sensing medium caused by the generation of biomolecule reaction.

In Fig. 1b, the phase sensitivity of SPR sensor comprises eight layers: SF11 prism, BK7 glass, titanium adhesion, Ag, ITO, BlueP/TMDCs, graphene, and sensing medium. For the first layer, the SF11 glass prism with the refractive index is given as [45]:

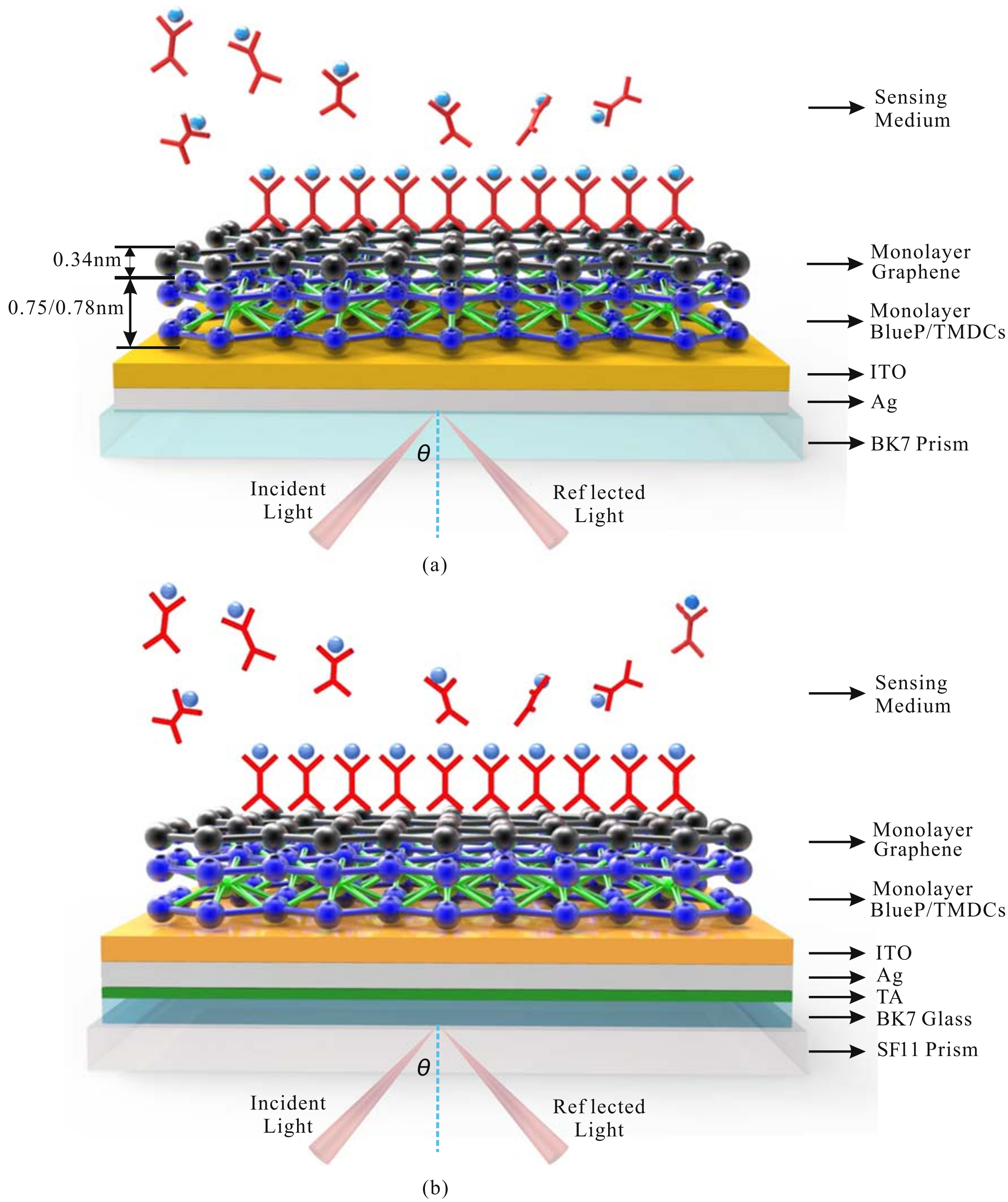

Fig. 1 Schematic diagram of the Ag-ITO-BlueP/TMDCs-garphene enhanced SPR sensor **a** angular sensitivity and **b** phase sensitivity

Table 1 The monolayer and refractive index of BlueP/TMDCs at the wavelength of 632.8 nm

Type of BlueP/TMDCs	Monolayer (nm)	Refractive index
BlueP/WS_2	0.75	2.480 + 0.170i
BlueP/MoS_2	0.75	2.810 + 0.320i
BlueP/WSe_2	0.78	2.680 + 0.220i
BlueP/$MoSe_2$	0.78	2.770 + 0.350i

$$n_{P1} = \sqrt{\frac{1.73759695\lambda^2}{\lambda^2-0.013188707}+\frac{0.313747346\lambda^2}{\lambda^2-0.0623068142}+\frac{1.89878101\lambda^2}{\lambda^2-155.23629}+1} \quad (5)$$

The second layer of BK7 glass is the same as BK7 glass in Fig. 1a. According to the experimental data of Palik, the composite refractive index at 632.8 nm was obtained [49]. Then, the remaining five layers are the same as the angular sensitivity.

SPR sensor in this work used the He-Ne laser beam (λ = 632.8 nm). The numerical simulation is calculated by MATLAB software. For the angular sensitivity, the thickness of BK7 glass and sensing medium are d_{A1} = 200 nm and d_{A6} = 100 nm, respectively. For the phase sensitivity, the thicknesses of SF11 glass, BK7 glass, titanium adhesion, and sensing medium are d_{P1} = 200 nm, d_{P2} = 100 nm, d_{P3} = 2.5 nm, and d_{P8} = 100 nm, respectively.

To study the SPR sensor performance, this paper uses the transfer matrix method (TMM) and the Fresnel equation based on the n-layer model. The reflectivity (R_p) of the p-polarization light is obtained as [52, 53]:

$$R_p = |r_p|^2 = \left| \frac{(M_{11} + M_{12}p_N)p_1 - (M_{21} + M_{22}p_N)}{(M_{11} + M_{12}p_N)p_1 + (M_{21} + M_{22}p_N)} \right|^2 \quad (6)$$

where $p_1$and p_N are the corresponding terms for the first and Nth layers, and M represents the layer structure combination of transfer matrix (TM).

The resonance angle is the incident angle corresponding to the minimum reflection ratio. Angular sensitivity (S_A) can be obtained by detecting the change of resonance angle ($\Delta\theta$) in the different refractive index of sensing media (Δn) [42]:

$$S_A = \frac{\Delta\theta}{\Delta n} \quad (7)$$

SPR only affects p-polarized light, so s-polarized light can be used as a reference signal for eliminating environmental noise to improve the stability and accuracy of SPR sensor in the whole measurement process. The differential phase (ψ_d) between p-polarization (ψ_p) and s-polarization (ψ_s) is shown as [40]:

$$\psi_d = |\psi_p - \psi_s| \quad (8)$$

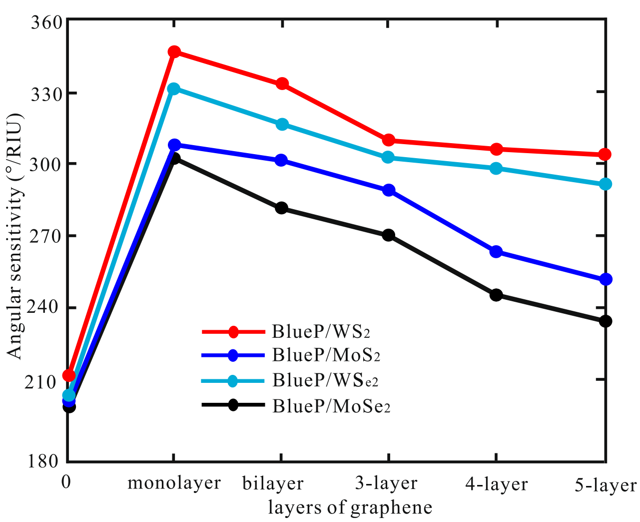

Fig. 2 Angular sensitivity of different graphene layers in Ag-ITO-BlueP/TMDCs (monolayer) structure

The SPR phase sensitivity (S_p) is defined as [46]:

$$S_p = \frac{\Delta\psi_d}{\Delta n_{bio}} \quad (9)$$

Results and Discussions

In past research, we can see that using relative bending index prism can obtain higher sensitivity. Therefore, due to the low refractive index of BK7 glass, it is selected as the coupling prism of the sensor. For the angular sensitivity, the change of refractive index of the sensing medium Δn is calculated to be 0.005 with the 632.8-nm beam as the incident light. In Fig. 2, the angular sensitivity of different layers of graphene in Ag-ITO-BlueP/TMDCs (monolayer) structure is obtained. We know that the graphene can get the best value in monolayer. With the increase of graphene layers, the angular sensitivity of Ag-ITO-BlueP/TMDCs (monolayer)-graphene structure is decreasing. Therefore, we only need to consider the condition with graphene monolayer.

In Fig. 3, the angular sensitivity with respect to the different BlueP/TMDCs layers with graphene monolayer is obtained. The optimized angular sensitivity with different layers of BlueP/TMDCs is shown in Table 2. Therefore, we can know that the angular sensitivity of Ag-ITO-graphene dielectric structure with the BlueP/TMDCs is greatly increased.

The highest angular sensitivity for the Ag-ITO-BlueP/TMDCs-graphene is shown as Table 3. When the BlueP/WS_2 is monolayer, the $\Delta\theta$ is 1.744° and the highest angular sensitivity is 348.8°/RIU. When the BlueP/MoS_2 is monolayer, the angular sensitivity is 309.6°/RIU. The BlueP/$MoSe_2$ is 8-layer, leading to the angular sensitivity of 341.2°/RIU. For the 7-layers of BlueP/WSe_2, the $\Delta\theta$ is 1.712° and the angular sensitivity is 342.4°/RIU. Therefore, we can know that the SPR sensor of Ag-ITO-BlueP/WS_2-graphene dielectric has the highest angular sensitivity of 348.8°/RIU.

The variation of the angular sensitivity with respect to the refractive index sensing medium is shown as Fig. 4. For the Ag-ITO-BlueP/WS_2-graphene structure (structure AI), when

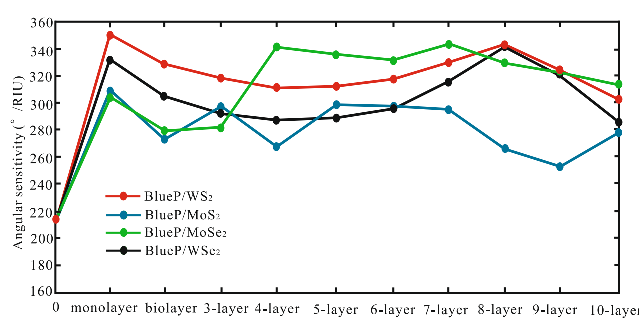

Fig. 3 Variation of the reflectance with respect to the layer of the BlueP/TMDCs with monolayer graphene

Table 2 The highest angular sensitivity for the Ag-ITO-BlueP/TMDCs-graphene structures

Type of BlueP/TMDCs	Thickness of Ag (nm)	Thickness of ITO (nm)	Optimized layers (*N*)	Graphene layers (*N*)	Change in resonance angle ($\Delta\theta$)	Angular sensitivity (°/RIU)
BlueP/WS_2	10	34	1	1	1.744	348.8
BlueP/WS_2	10	33	2	1	1.642	328.4
BlueP/WS_2	10	31	3	1	1.590	318.0
BlueP/$MoSe_2$	9	27	4	1	1.708	341.6
BlueP/$MoSe_2$	9	24	5	1	1.674	334.8
BlueP/$MoSe_2$	9	22	6	1	1.644	328.8
BlueP/$MoSe_2$	9	19	7	1	1.712	342.4
BlueP/WS_2	10	24	8	1	1.722	344.4
BlueP/WS_2	10	19	9	1	1.640	328.0
BlueP/$MoSe_2$	9	17	10	1	1.579	315.8

the graphene is monolayer and n_{A6} is 1.330, the highest angular sensitivity of 348.8°/RIU is obtained. With the increasing of n_{A6}, the angular sensitivity of structure AI is gradually decreasing. When the n_{A6} is 1.336, the angular sensitivity of 301°/RIU is obtained. For the Ag-ITO-graphene structure (structure AII), when the graphene is monolayer and n_{A6} is 1.330, the angular sensitivity is 217.6°/RIU. With the increasing of n_{A6}, the angular sensitivity of structure AII is decreasing. In the $n_{A6} = 1.336$, the angular sensitivity of 207.6°/RIU is obtained. For the Ag-ITO structure (structure AIII), when the thicknesses of Ag and ITO are 46 nm and 12 nm, and n_{A6} is 1.330, the angular sensitivity of 168.4°/RIU is gained. With the increasing of n_{A6}, the angular sensitivity of structure AIII is gradually increasing. In the $n_{A6} = 1.336$, the angular sensitivity of 177°/RIU is obtained. For the traditional SPR sensor with Ag, the angular sensitivity is 123.4°/RIU by the thickness of Ag at 53 nm and $n_{A6} = 1.330$. With the increase of n_{A6}, the angular sensitivity increases gradually. At the $n_{A6} = 1.336$, the angular sensitivity reaches 127°/RIU. Therefore, the angular sensitivity of structure AI is 1.60 times higher than that of structure AII and 1.68 times higher than that of structure AIII and 2.83 times higher than that of traditional SPR sensor.

Then, the phase sensitivity is discussed. In order to analysis of phase sensitivity, the thickness of Ag is fixed at 21 nm. In Fig. 5, the phase sensitivity with different layers of BlueP/TMDCs for diffident graphene is obtained. The highest phase sensitivity for SPR sensor with Ag-ITO-BlueP/TMDCs (1-5)-graphene (1-4) dielectric structure is summarized in Table 4. It can be seen that when the BlueP/WSe_2 is monolayer and graphene is bilayer, the highest phase sensitivity of 3.603×10^6 deg/RIU is obtained. Therefore, the BlueP/TMDCs plays an important role in phase sensitivity for SPR sensor.

The optimum layer, graphene layers, the thickness of ITO, and highest phase sensitivity for SPR sensor with Ag-ITO-BlueP/TMDCs-graphene dielectric structure are shown in Table 5. The order of phase sensitivity from high to low is BlueP/WSe_2, BlueP/MoS_2, BlueP/$MoSe_2$, and BlueP/WS_2, respectively.

For the Ag-ITO-BlueP/WSe_2-graphene heterostructures, when the thicknesses of WSe_2 and graphene are monolayer and bilayer, respectively, the maximum phase sensitivity value 3.603×10^6 deg/RIU is obtained. Therefore, phase sensitivity of Ag-ITO structure (structure PIII), Ag-ITO-graphene (bilayer) structure (structure PII), and Ag-ITO-BlueP/WSe_2 (monolayer)-graphene (bilayer) structure (structure PI) dielectric structure is discussed in Fig. 6. In Fig. 6a, when the refractive index sensing medium (n_{P8}) is 1.330, the structure PI has the maximum phase change at $\Delta\theta$ of 48.40°, the structure PII has phase change at $\Delta\theta$ of 48.42°, and the structure PIII has the phase change at $\Delta\theta$ of 48.45°. From Fig. 6b, we can know that the structure PII and structure PIII are 1.295×10^6 deg/RIU and 6.269×10^5 deg/RIU at the $n_{P8} = 1.330$, respectively. When $n_{P8} = 1.331$, the structure PI is 1.671×10^6 deg/RIU, the structure PII is 1.399×10^6 deg/RIU, and

Table 3 The highest angular sensitivity for the Ag-ITO-BlueP/TMDCs-graphene (monolayer)

Type of BlueP/TMDCs	Thickness of Ag (nm)	Thickness of ITO (nm)	Optimized layers (*N*)	Change in resonance angle ($\Delta\theta$)	Angular sensitivity (°/RIU)
BlueP/WS_2	10	34	1	1.744	348.8
BlueP/MoS_2	10	34	1	1.548	309.6
BlueP/WSe_2	10	21	8	1.706	341.2
BlueP/$MoSe_2$	9	19	7	1.712	342.4

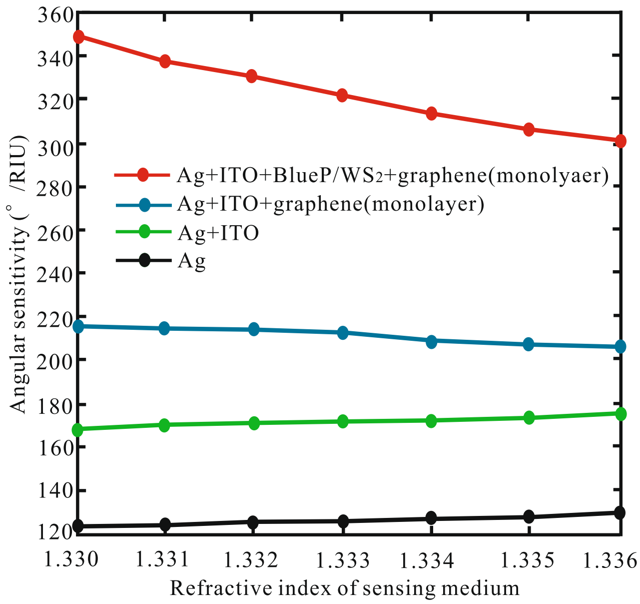

Fig. 4 Variation of the angular sensitivity with respect to the refractive index sensing medium

the structure PIII is 7.788 × 10^6 deg/RIU. In n_{P8} = 1.331, the structure PI has decreased significantly compared with n_{P8} = 1.330. With the increase of n_{P8}, there is a small fluctuation of phase sensitivity, structure PI is kept at 1.580 × 10^6 deg/RIU to 1.770 × 10^6 deg/RIU, structure PII is kept at 8.960 × 10^5 deg/RIU to 1.260 × 10^6 deg/RIU, and structure PIII is kept at 6.850 × 10^5 deg/RIU to 8.120 × 10^6 deg/RIU. Therefore, the phase sensitivity of structure PI is 2.78 higher than that of structure PII and 4.16 times higher than that of structure PIII.

Comparative Analysis

In order to compare the results of previous studies, Table 6 summarizes the performance of metal-2D material-assisted SPR sensor made. In the designed SPR sensor, the angular and phase sensitivity have been significantly improved.

First, we discuss the angular sensitivity. In reference [40], the angular sensitivity of 155.68°/RIU is obtained by Au-

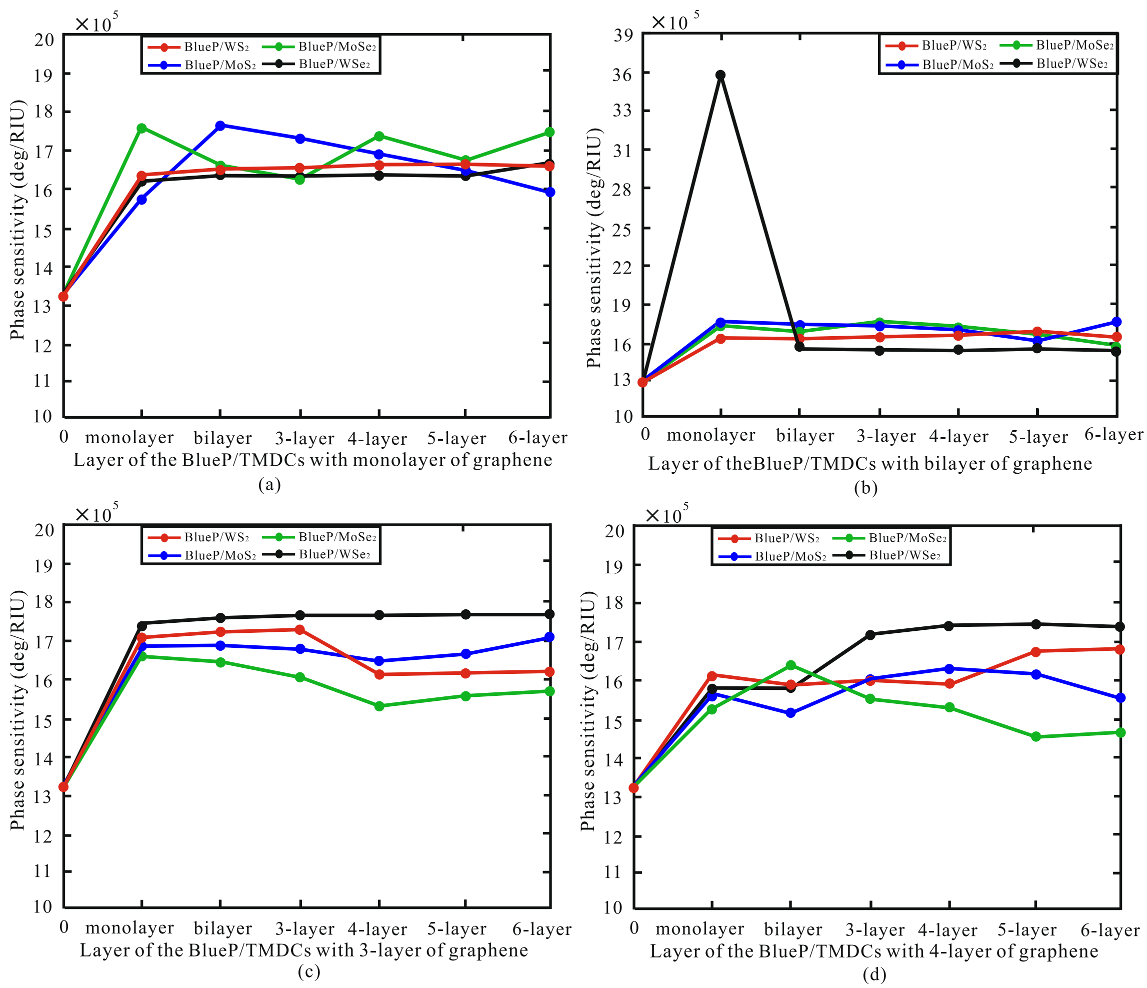

Fig. 5 The phase sensitivity with different layers of BlueP/TMDCs: **a** monolayer of graphene, **b** bilayer of graphene, **c** 3-layer of graphene, **d** 4-layer of graphene

Table 4 The highest phase sensitivity for Ag-ITO-BlueP/TMDCs (1-5)-graphene (1-4) dielectric structure

Type of BlueP/TMDCs	The thickness of ITO (nm)	Optimized layers (*N*)	Graphene layers (*N*)	Phase sensitivity (deg/RIU)
BlueP/WS_2	192	5	1	1.700×10^6
BlueP/MoS_2	191	2	1	1.760×10^6
BlueP/WSe_2	188	6	1	1.632×10^6
BlueP/$MoSe_2$	192	1	1	1.754×10^6
BlueP/WS_2	190	5	2	1.725×10^6
BlueP/MoS_2	185	6	2	1.757×10^6
BlueP/WSe_2	191	1	2	3.603×10^6
BlueP/$MoSe_2$	188	3	2	1.731×10^6
BlueP/WS_2	188	3	3	1.722×10^6
BlueP/MoS_2	184	6	3	1.706×10^6
BlueP/WSe_2	185	6	3	1.769×10^6
BlueP/$MoSe_2$	190	1	3	1.671×10^6
BlueP/WS_2	184	6	4	1.688×10^6
BlueP/MoS_2	186	4	4	1.624×10^6
BlueP/WSe_2	185	4	4	1.731×10^6
BlueP/$MoSe_2$	188	2	4	1.659×10^6

silicon-WS_2 dielectric structure. In reference [41], when BP of 2D material replaces silicon, the angular sensitivity is improved to 187°/RIU. We can find that 2D material can improve the performance of SPR sensor. In reference [42], the angular sensitivity of 219.4°/RIU is obtained by Ag-ITO-WS_2 dielectric structure. In reference [43], when BP and WSe_2 replace ITO and WS_2, respectively, the angular sensitivity is improved to 279°/RIU. For reference [44], the angular sensitivity of 315.5°/RIU is gained by WS_2-Al-WS_2-graphene dielectric structure. However, in reference [48], when the BlueP/MoS_2 is added to Au and silicon, the angular sensitivity increases to 230.66°/RIU. Compared with reference [40], the

Table 5 The highest phase sensitivity for Ag-ITO-BlueP/TMDCs-graphene dielectric structure

Type of BlueP/TMDCs	The thickness of Ag (nm)	The thickness of ITO (nm)	Optimized layers (*N*)	Graphene layers (*N*)	Phase sensitivity (deg/RIU)
BlueP/WS_2	21	188	3	3	1.722×10^6
BlueP/MoS_2	21	191	2	1	1.760×10^6
BlueP/WSe_2	21	191	1	2	3.603×10^6
BlueP/$MoSe_2$	21	192	1	1	1.754×10^6

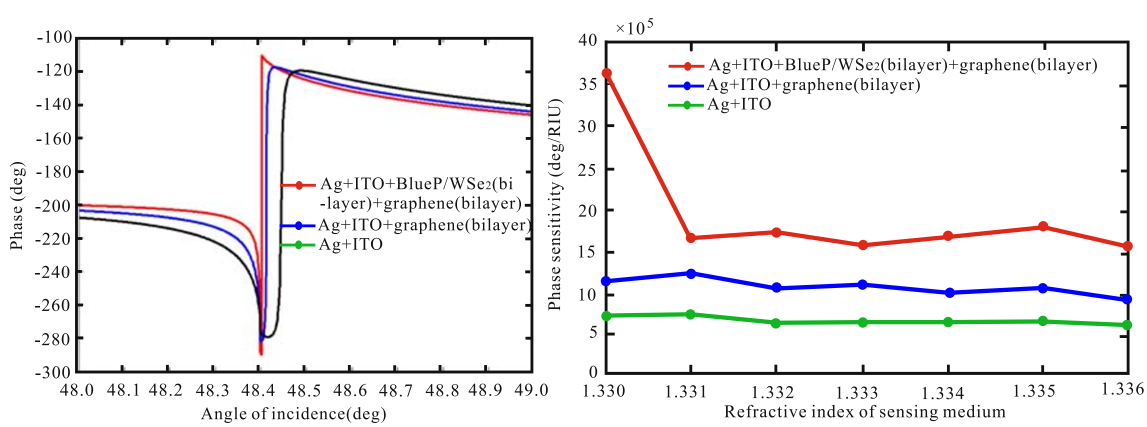

Fig. 6 **a** The phase sensitivity of structure PIII, structure PII, and structure PI with $n_{P8} = 1.330$. **b** Variation of the phase sensitivity with respect to the refractive index sensing medium

Table 6 Comparison of angular and phase sensitivity

Multilayer structure	Metal (nm)	ITO (nm)	TMDCs (layers)	Graphene (layers)	Angular Sensitivity (°/RIU)	Phase Sensitivity (deg/RIU)	References
Au-silicon-WS_2	35	-	Monolayer	-	155.68	-	[40]
Au-BP-WS_2	25	-	Monolayer	-	187	-	[41]
Ag-ITO-WS_2	62	5	3-layer	-	219.4	-	[42]
Ag-BP-WSe_2	50	-	Bilayer	-	279	-	[43]
WS_2-Al-WS_2-graphene	36	-	7-layer	Monolayer	315.5	-	[44]
Au-silicon-BlueP/MoS_2	20	-	Monolayer	-	230.66		[48]
Ag-ITO-BlueP/WS_2-graphene	10	34	Monolayer	Monolayer	348.4		This work
Au-graphene-MoS_2	45	-	3-layer	Monolayer	-	8.185×10^4	[45]
Ag-ITO-WS_2	18	190	Monolayer	-	-	1.711×10^6	[46]
Cu-ITO-$MoSe_2$	23	214	5-layer	-	-	1.821×10^6	[42]
Ag-ITO-BlueP/WSe_2-graphene	21	191	Monolayer	Bilayer	-	3.603×10^6	This work

performance of BlueP/TMDCs is much better than that of TMDCs. In this work, when the ITO, BlueP/WSe_2, and graphene are added to the SPR sensor, the angular sensitivity is enhanced to 348.4°/RIU. Subsequently, the phase sensitivity is discussed. In reference [45], when two kinds of 2D materials are added to the metal, the phase sensitivity of 8.185×10^4 deg/RIU is gained by Au-graphene-MoS_2 dielectric structure. In references [46], when the ITO and WS_2 replace BP, the phase sensitivity is enhanced to 1.711×10^6 deg/RIU. In reference [42], the phase sensitivity value of Cu-ITO-$MoSe_2$ is 1.821×10^6 deg/RIU. But, in this work, after adding ITO on the basis of two kinds of 2D materials, the phase sensitivity value of Ag-ITO-BlueP/WSe_2-graphene structure is 3.603×10^6 deg/RIU. Therefore, we can know that the BlueP/TMDCs can improve performance of SPR sensor.

Conclusion

In this work, a novel Ag-ITO-BlueP/TMDCs-graphene structures SPR sensor for higher precision biological instruments is optimized and compared. First, we use a different layer of BlueP/TMDCs and graphene to coat on the Ag and ITO film to enhance the angular sensitivity, and the result shows that the angular sensitivity can be increased to 348.4°/RIU by the Ag-ITO-BlueP/WS_2-graphene dielectric structure. The angular sensitivity of Ag-ITO-BlueP/WS_2-graphene structure is 1.60 times higher than that of Ag-ITO-graphene structure and 1.68 times higher than that of Ag-ITO structure and 2.83 times higher than traditional SPR sensor of Ag film. Secondly, the SPR sensor based on Ag-ITO-BlueP/WSe_2-graphene dielectric structure with phase sensitivity of 3.603×10^6 deg/RIU shows best performance, which the BlueP/WSe_2 is monolayer and graphene is bilayer. The phase sensitivity of Ag-ITO-BlueP/WSe_2-graphene structure is 2.78 higher than that of Ag-ITO-graphene structure and 4.16 times higher than that of Ag-ITO structure. Therefore, the sensor of Ag-ITO-BlueP/TMDCs-graphene structure proposed in this paper may provide new ideas for design of ultrasensitive SPR sensor.

Funding Information This work was partially supported by Wuhan Science and Technology Bureau under grant (2018010401011297) and the Fundamental Research Funds for the Central Universities, China University of Geosciences (Wuhan) (162301132703, G1323511665).

References

1. Xue TY, Qia K, Hu CQ (2019) Novel SPR sensing platform based on superstructure MoS_2 nanosheets for ultrasensitive detection of mercury ion. Sens Actuators B Chem 284:589–594
2. Taylor AD, Ladd J, Yu QM, Chen SF, Homola J, Jiang SY (2006) Quantitative and simultaneous detection of four foodborne bacterial pathogens with a multi-channel SPR sensor. Biosens Bioelectron 22(5):752–758
3. Lautner G, Balogh Z, Bardóczy V, Mészáros T, Gyurcsányi RE (2010) Aptamer-based biochips for label-free detection of plant virus coat proteins by SPR imaging. Analyst 135(5):918–926
4. Wu L, Chu HS, Koh WS, Li EP (2010) Highly sensitive graphene biosensors based on surface plasmon resonance. Opt Express 18(14):14395–14400
5. Raed A, Mehrdad I, Mustafa Y (2019) A short review on the role of the metal-graphene hybrid nanostructure in promoting the localized surface plasmon resonance sensor performance. Sensors 19(4):862
6. Kaushik S, Tiwari UK, Deep A, Sinha RK (2019) Two-dimensional transition metal dichalcogenides assisted biofunctionalized optical fiber SPR biosensor for efficient and rapid detection of bovine serum albumin. SCI REP-UK 9:6987
7. Yakes BJ, Buijs J, Elliott CT (2016) Surface plasmon resonance biosensing: approaches for screening and characterizing antibodies for food diagnostics. Talanta 156:55–63
8. Kim J, Hong S, Choi Y (2019) Sensitive detection of formaldehyde gas using modified dandelion-like SiO_2/Au film and surface plasmon resonance system. J Nanosci Nanotechno 19(8):4807–4811
9. Zeng SW, Sreekanth KV, Shang JZ, Yu T, Chen CK, Yin F, Baillargeat D, Coquet P, Ho HP, Kabashin AV, Yong KT (2015)

Graphene-gold metasurface architectures for ultrasensitive plasmonic biosensing. Adv Mater 27(40):6163–6169
10. Hottin J, Wijaya E, Hay L, Maricot S, Bouazaoui M, Vilcot JP (2013) Comparison of gold and silver/gold bimetallic surface for highly: sensitive near-infrared SPR sensor at 1550 nm. Plasmonics 8(2):619–624
11. Ruan B, Qi Y, Zhu JQ, Wu LM, Guo J, Dai XY, Xiang YJ (2018) Improving the performance of an SPR biosensor using long-range surface plasmon of Ga-doped zinc oxide. Sensors 8(7):2098
12. Chen X, Zheng ZF, Ke XB, Jaatinen E, Xie TF, Wang DJ, Guo C, Zhao JC, Zhu HY (2010) Supported silver nanoparticles as photocatalysts under ultraviolet and visible light irradiation. Green Chem 12(3):414–419
13. Han L, Ding HF, Huang TY, Wu X, Chen B, Ren K, Fu S (2018) Broadband optical reflection modulator in indium-tin-oxide-filled hybrid plasmonic waveguide with high modulation depth. Plasmonics 13(4):1309–1314
14. Wu L, Guo J, Dai X, Xiang Y, Fan D (2017) Sensitivity enhanced by MoS_2–graphene hybrid structure in guided-wave surface plasmon resonance biosensor. Plasmonics 13(1):281–285
15. Liu C, Liu QG, Hu XT (2014) SPR phase detection for measuring the thickness of thin metal films. Opt Express 22(7):7574–7580
16. Saigusa M, Tsuboi K, Konosu Y, Ashizawa M, Tanioka A, Matsumoto H (2015) Highly sensitive local surface plasmon resonance in anisotropic Au nanoparticles deposited on nanofibers. J Nanomater 2015:1–8
17. Liu Y, Huang CZ (2013) Screening sensitive nanosensors via the investigation of shape-dependent localized surface plasmon resonance of single Ag nanoparticles. Nanoscale 5:7458–7466
18. Chung HY, Chen CC, Wu PC, Tseng ML, Lin WC, Chen CW, Chiang HP (2014) Enhanced sensitivity of surface plasmon resonance phase-interrogation biosensorby using oblique deposited silver nanorods. Nanoscale Res Lett 9:476–480
19. Su W, Zheng G, Li X (2012) Design of a highly sensitive surface plasmon resonance sensor using aluminum based diffraction grating. Opt Commun 285:4603–4607
20. Sang XZ, Zhang DW (2016) Research on the SPR properties of copper thin film with regulation of titanium dioxide. Spectrosc Spectr Anal 36(7):2027–2030
21. Leong KH, Gan BL, Ibrahim S, Saravanan P (2014) Synthesis of surface plasmon resonance (SPR) triggered Ag/TiO_2 photocatalyst for degradation of endocrine disturbing compounds. Appl Surf Sci 319:128–135
22. Usov OA, Nashchekin AV (2009) SPR of Ag nanoparticles in photothermochromic glasses. Proc SPIE-Int Soc Opt Eng 7394: 73942J–73942J-6
23. Kanehara M, Koike H, Yoshinaga T, Teranishi T (2009) Indium tin oxide nanoparticles with compositionally tunable surface plasmon resonance frequencies in the near-IR region. J Am Chem Soc 131(49):17736–17737
24. Kakil SA, Sabr BN, Hana LS, Abbas AH, Hussin SY (2018) Effects of a low dose of gamma radiation on the morphology, and the optical and the electrical properties of an ITO thin film as an electrode for solar cell applications. J Korean Phys Soc 72(5):561–569
25. Farhan MS, Zalnezhad E, Bushroa AR, Sarhan AAD (2013) Electrical and optical properties of indium-tin oxide (ITO) films by in-assisted deposition (IAD) at room temperature. Int J Precision Eng Manuf 14:1465–1469
26. Tuo YF, Wu YP, Huang M, Wang K, Huang Y, Zhou ZH, Shen SZ (2015) The surface plasmon resonance absorption of indium tin oxide nanoparticles and its control. Adv Mater Res 1118:160–165
27. Du J, Chen X, Liu C, Ni J, Hou G, Zhao Y, Zhang X (2014) Highly transparent and conductive indium tin oxide thin films for solar cells grown by reactive thermal evaporation at low temperature. Appl Phys A Mater Sci Process 117:815–822
28. Li ZQ, He JH, Wang YJ, Feng DD, Gu ED, Li WC (2012) Self-referenced SPR sensor based on Au/ITO Nanocomposite. Acta Photonica Sinica 45(12):1228002-1–1228002-7
29. Szunerits S, Castel X, Boukherroub R (2008) Surface plasmon resonance investigation of silver and gold films coated with thin indium tin oxide layers: influence on stability and sensitivity. J Phys Chem C 112(40):15813–15817
30. Gan SM, Menon PS, Mohamad NR, Jamil NA, Majlis BY (2019) FDTD simulation of Kretschmann based Cr-Ag-ITO SPR for refractive index sensor. Materials Today: Proceedings, 7: 668–674
31. Sharma NK, Yadav S, Sajal V (2014) Theoretical analysis of highly sensitive prism based surface plasmon resonance sensor with indium tin oxide. Opt Commun 318:74–78
32. Zeng S, Baillargeat D, Ho HP, Yong KT (2014) Nanomaterials enhanced surface plasmon resonance for biological and chemical sensing applications. Chem Soc Rev 43:3426–3452
33. Zhu YW, Murali S, Cai WW, Li XS, Suk JW, Potts JR, Ruoff RS (2010) Graphene and graphene oxide: synthesis, properties, and applications. Adv Mater 22(35):3906–3924
34. Subramanian P, Lesniewski A, Kaminska I, Vlandas A, Vasilescu A, Niedziolka-Jonsson J (2013) Lysozyme detection on aptamer functionalized graphene-coated SPR interfaces. Biosens Bioelectron 50:239–243
35. Simsek E (2013) Improving tuning range and sensitivity of localized SPR sensors with graphene. IEEE Photon Technol Lett 25(9): 867–870
36. Chiu NF, Huang TY, Lai HC, Liu KC (2014) Graphene oxide-based SPR biosensor chip for immunoassay applications. Nanoscale Res Lett 9:445
37. Said FA, Menon PS, Rajendran V, Sharri S, Majlis BY (2017) Investigation of graphene-on-metal substrates for SPR-based sensor using finite-difference time domain. Iet Nanobiotechnology 11(8): 981–986
38. Wang QH, Kalantarzadeh K, Kis A, Coleman JN, Strano MS (2012) Electronics and optoelectronics of two-dimensional transition metal dichalcogenides. Nat Nanotechnol 7(11):699–712
39. Liu Y, Duan XD, Huang Y, Duan XF (2018) Two-dimensional transistors beyond graphene and TMDCs. Chem Soc Rev 47(16): 6388–6409
40. Ouyang QL, Zeng SW, Dinh XQ, Coquet P, Yong KT (2016) Sensitivity enhancement of transition metal dichalcogenides/silicon nanostructure-based surface plasmon resonance biosensor. SCI REP-UK 6:28190
41. Meshginqalam B, Barvestani J (2018) Performance enhancement of SPR biosensor based on phosphorene and transition metal dichalcogenides for sensing DNA hybridization. IEEE Sensors J 18(18):7537–7543
42. Han L, He XJ, Ge LC, Huang TY, Ding HF, Wu C (2019) Comprehensive study of performance SPR biosensor based on metal-ITO-graphene/TMDCs hybrid multilayer. Plasmonics. https://doi.org/10.1007/s11468-019-01004-w
43. Wu LM, Guo J, Wang QK, Lu SB, Dai XY, Xiang YJ, Fan DY (2017) Sensitivity enhancement by using few-layer black phosphorus-graphene/TMDCs heterostructure in surface plasmon resonance biochemical sensor. Sens Actuators B Chem 249:542–548
44. Zhao X, Huang TY, Perry SP, Wu X, Huang P, Pan JX, Wu YH, Cheng Z (2018) Sensitivity enhancement in surface plasmon resonance biochemical sensor based on transition metal dichalcogenides/graphene heterostructure. Sensors 18(7):2056
45. Zeng SW, Hu SY, Xia J, Anderson T, Dinh XQ, Meng XM, Coquet P, Yong KT (2015) Graphene–MoS_2 hybrid nanostructures enhanced surface plasmon resonance biosensors. Sens Actuators B Chem 207:801–810
46. Han L, Zhao X, Huang TY, Ding HF, Wu C (2019) Comprehensive study of phase-sensitive SPR sensor based on metal-ITO hybrid

multilayer. Plasmonics 14:1743–1750. https://doi.org/10.1007/s11468-019-00968-z
47. Peng Q, Wang Z, Sa B, Wu B, Sun Z (2016) Electronic structures and enhanced optical properties of blue phosphorene/transition metal dichalcogenides van der Waals heterostructures. Sci Rep 6: 31994
48. Srivastava A, Prajapati YK (2019) Performance analysis of silicon and blue phosphorene/MoS_2 hetero-structure based SPR sensor. Photonic Sensors 9(3):284–292
49. Palik ED (1985) Handbook of optical constants of solids. Academic, New York
50. Gupta BD, Sharma AK (2005) Sensitivity evaluation of a multi-layered surface plasmon resonance-based fiber optic sensor: a theoretical study. Sens Actuators B Chem 107:40–46
51. Han L, Wu C (2019) A phase-sensitivity-enhanced surface plasmon resonance biosensor based on ITO-graphene hybrid structure. Plasmonics 14(4):901–906
52. Sreekanth KV, Zeng S, Yong KT, Yu T (2013) Sensitivity enhanced biosensor using graphene-based one-dimensional photonic crystal, Sens. Actuators B Chem 182:424–428
53. Roy K, Padmanabhan M, Goswami S, Sai TP, Ramalingam G, Raghavan S, Ghosh A (2013) Graphene-MoS_2 hybrid structures for multifunctional photoresponsive memory devices. Nat Nanotechnol 8:826–830

Publisher's Note Springer Nature remains neutral with regard to jurisdictional claims in published maps and institutional affiliations.